DOI:
10.1002/jmri.26869

Document Version
Publisher's PDF, also known as Version of record

FASt Single-Breathhold 2D Multislice Myocardial T_1 Mapping (FAST1) at 1.5T for Full Left Ventricular Coverage in Three Breathholds

Li Huang, PhD,[1] Radhouene Neji, PhD,[1,2] Muhummad Sohaib Nazir, MD,[1] John Whitaker, MD,[1] Phuoc Duong, MD,[1] Fiona Reid, PhD,[3] Filippo Bosio, BSc,[1] Amedeo Chiribiri, PhD, MD,[1] Reza Razavi, PhD, MD,[1] and Sébastien Roujol, PhD[1]*

Background: Conventional myocardial T_1 mapping techniques such as modified Look–Locker inversion recovery (MOLLI) generate one T_1 map per breathhold. T_1 mapping with full left ventricular coverage may be desirable when spatial T_1 variations are expected. This would require multiple breathholds, increasing patient discomfort and prolonging scan time.
Purpose: To develop and characterize a novel FASt single-breathhold 2D multislice myocardial T_1 mapping (FAST1) technique for full left ventricular coverage.
Study Type: Prospective.
Population/Phantom: Numerical simulation, agarose/$NiCl_2$ phantom, 9 healthy volunteers, and 17 patients.
Field Strength/Sequence: 1.5T/FAST1.
Assessment: Two FAST1 approaches, FAST1-BS and FAST1-IR, were characterized and compared with standard 5-(3)-3 MOLLI in terms of accuracy, precision/spatial variability, and repeatability.
Statistical Tests: Kruskal-Wallis, Wilcoxon signed rank tests, intraclass correlation coefficient analysis, analysis of variance, Student's *t*-tests, Pearson correlation analysis, and Bland–Altman analysis.
Results: In simulation/phantom, FAST1-BS, FAST1-IR, and MOLLI had an accuracy (expressed as T_1 error) of 0.2%/4%, 6%/9%, and 4%/7%, respectively, while FAST1-BS and FAST1-IR had a precision penalty of 1.7/1.5 and 1.5/1.4 in comparison with MOLLI, respectively. In healthy volunteers, FAST1-BS/FAST1-IR/MOLLI led to different native myocardial T_1 times (1016 $\pm$ 27 msec/952 $\pm$22 msec/987 $\pm$ 23 msec, $P < 0.0001$) and spatial variability (66 $\pm$ 10 msec/57 $\pm$ 8 msec/46 $\pm$ 7 msec, $P < 0.001$). There were no statistically significant differences between all techniques for T_1 repeatability ($P = 0.18$). In vivo native and postcontrast myocardial T_1 times in both healthy volunteers and patients using FAST1-BS/FAST1-IR were highly correlated with MOLLI (Pearson correlation coefficient ≥0.93).
Data Conclusion: FAST1 enables myocardial T_1 mapping with full left ventricular coverage in three separated breathholds. In comparison with MOLLI, FAST1 yield a 5-fold increase of spatial coverage, limited penalty of T_1 precision/spatial variability, no significant difference of T_1 repeatability, and highly correlated T_1 times. FAST1-IR provides improved T_1 precision/spatial variability but reduced accuracy when compared with FAST1-BS.
Level of Evidence: 1
Technical Efficacy: Stage 3

J. MAGN. RESON. IMAGING 2019.

ALTERATION OF NATIVE MYOCARDIAL T_1 times has been observed in the presence of a variety of heart diseases such as acute and chronic myocardial infarction, myocarditis, amyloidosis, or Anderson–Fabry disease.[1] Myocardial T_1 mapping techniques enable pixelwise quantification of myocardial T_1 times,[2] which has promising value for diagnosis and prognosis.[1]

View this article online at wileyonlinelibrary.com. DOI: 10.1002/jmri.26869

Received May 16, 2019, Accepted for publication Jul 2, 2019.

*Address reprint requests to: S.R., 3rd Floor, Lambeth Wing, St Thomas' Hospital, Westminster Bridge Road, London, SE1 7EH, UK. E-mail: sebastien.roujol@kcl.ac.uk

From the [1]The School of Biomedical Engineering and Imaging Sciences, Faculty of Life Sciences and Medicine, King's College London, London, UK; [2]MR Research Collaborations, Siemens Healthcare Limited, Frimley, UK; and [3]School of Population Health and Environmental Sciences, Faculty of Life Sciences and Medicine, King's College London, London, UK

Additional supporting information may be found in the online version of this article

The desired spatial coverage of myocardial T_1 mapping (single-slice vs. multislice vs. full left ventricular [LV] coverage) may depend on the cardiac conditions, as stated by an expert consensus statement.[1] Full LV coverage may be beneficial when spatial variations in LV wall thickness and/or fibrosis are expected, such as in the presence of hypertrophic cardiomyopathy[3] or chronic myocardial infarction.[4,5]

Several methods have been proposed for myocardial T_1 mapping, including techniques based on inversion,[2,6] saturation,[7] or hybrid preparation pulses.[8] In these approaches, multiple images with different T_1-weightings are acquired and fit in a pixelwise manner to a physical model of the MR signal evolution.[2] Inversion recovery (IR)-based approaches such as modified Look–Locker inversion recovery (MOLLI)[2] are commonly used due to their high precision, reproducibility, and map quality.[9–12] In these techniques, multiple (usually 7–13) 2D single-shot electrocardiogram (ECG)-triggered images of the same slice are acquired at different inversion times (TIs) in a single breathhold and used to generate one T_1 map. In these conditions, myocardial T_1 mapping with full LV coverage requires repeated breathheld acquisitions, each for one slice, thus increasing patient discomfort, prolonging scan time, and resulting in potential slice misalignment if 3D processing is necessary.

3D or advanced 2D multislice techniques can be used to achieve native myocardial T_1 mapping with full LV coverage.[13–20] 3D breathheld myocardial T_1 mapping approaches may need to compromise between spatial resolution and/or artifact level due to limited breathhold duration and limited acquisition window within the cardiac cycle.[13,18] On the other hand, 3D[14,15,17,19,20] and 2D multislice[16] free-breathing myocardial T_1 mapping require long scan times and advanced motion correction strategies, which can result in reduced map quality and increased intersegment variability compared with standard breathheld techniques such as MOLLI.[17]

In this work, we sought to develop and characterize a novel FASt single-breathhold 2D multislice myocardial T_1 mapping (FAST1) for myocardial T_1 mapping with full LV coverage in three breathholds at 1.5T.

Materials and Methods

Pulse Sequence

The FAST1 pulse sequence diagram is illustrated in Fig. 1, where five T_1 maps are acquired in one breathhold. A slice-selective inversion pulse (phase-modulated hyperbolic secant) is applied in the first heartbeat (HB). Two ECG-triggered single-shot images of the same slice are then acquired over the first and second HBs at TIs of TI_1 and TI_2, respectively. The delay time between the slice-selective inversion pulse and the first image (TI_1) is minimized to reduce the impact of motion. This imaging block is then repeated five times for different slices within the same breathhold.

To reduce the slice mismatch in the presence of residual motion occurring between the inversion and imaging, the ratio of inversion to imaging slice thickness was increased from one to a factor of R_{THK}. Furthermore, the five imaging blocks were acquired in a slice-interleaved fashion using the following slice order (#1, #3, #5, #2, #4) and a slice gap (twice the imaging slice thickness in this work) to minimize slice crosstalk.

To allow for large R_{THK} values and thus improved robustness against motion while minimizing slice crosstalk, recovery HBs were inserted between the third and fourth imaging blocks (between slices #5 and #2, respectively). The number of recovery HBs (N_R) is adjusted based on each subject's heart rate (HR) to ensure quasi full

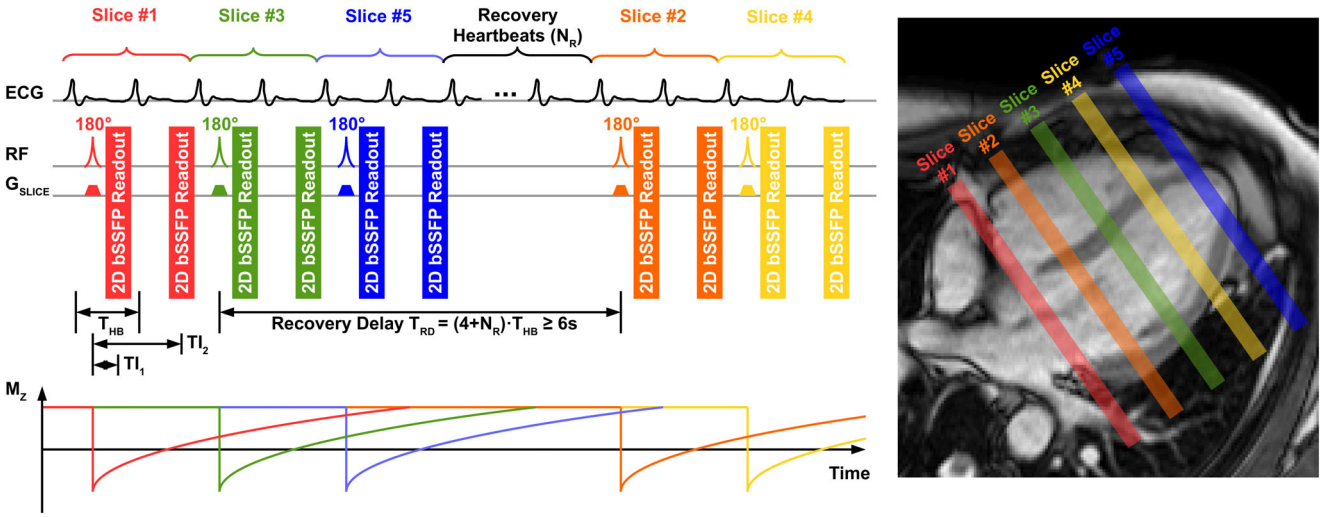

FIGURE 1: FAST1 sequence diagram and acquisition scheme. Five T_1 maps are acquired in one breathhold, each based on a two-heartbeat imaging block including a slice-selective inversion pulse and the acquisition of two ECG-triggered single-shot images. Minimal inversion time is used for each imaging block to reduce the impact of cardiac motion between the slice-selective inversion pulse and the first image acquisition. An inversion slice thickness larger than the imaging slice thickness is used to minimize the impact of cardiac motion. Recovery heartbeats are introduced between the third and fourth imaging blocks to minimize potential slice crosstalk between the slice-selective inversion pulses. In the physiological HR range (50–110 bpm), the corresponding nominal breathhold duration is 9–13 sec.

recovery of the longitudinal magnetization of the last two slices (slices #2, #4) before application of their associated slice-selective inversion pulses. This adjustment is achieved based on a worst-case scenario defined as one slice-selective inversion pulse in the first three imaging blocks (for slices #1, #3, or #5) fully inverted one of its adjacent slices (slices #2 or #4). Considering a normal native myocardial T_1 at 1.5T (~1200 msec), recovery HBs were added to ensure a minimum delay of five times the native myocardial T_1 time between the inversion pulses for two adjacent slices (ie, $T_{RD} \geq 6$ sec). As an example, with an HR of 60 bpm, two recovery HBs were used (ie, $N_R = 2$). In the physiological HR range (50–110 bpm), the corresponding nominal breathhold duration is 9–13 sec.

T_1 Map Reconstruction

T_1 map reconstruction was performed using an exhaustive search over a signal dictionary. Two models were developed and evaluated for the creation of the signal dictionary using Bloch equations simulation (BS) of the pulse sequence and an IR-based model. The corresponding reconstructions are thereafter referred to as FAST1-BS and FAST1-IR, respectively. Each model was created using a T_1 range of 1–4000 msec in steps of 1 msec.

BS MODEL. The signal dictionary was generated using Bloch equations simulation of FAST1. The signal of each T_1-weighted image was simulated as the transversal magnetization at the *k*-space center (ie, TI_1 and TI_2). An initial longitudinal magnetization of 1 was used. T_1-dependent slice profiles of the inversion pulse (phase-modulated hyperbolic secant) and the excitation pulse (nonmodulated Hann-filtered sinc) were integrated. T_1-dependent slice profiles were estimated using Bloch equations simulation of each pulse with a myocardial T_2 = 45 msec and B0/B1 inhomogeneities [80%,100%]/[–150,150] Hz in steps of 1%/10 Hz. T_1-dependent effective flip angles were approximated based on the average longitudinal magnetization over the slice profiles and all simulated T_2/B0/B1 regimes.

IR MODEL. The dictionary was created using a previously proposed normalized one-parameter model[21] defined as:

$$S(t) = 1 - (1 + \delta)e^{-t/T1}, \quad (1)$$

where δ is a constant term representing the inversion factor of the inversion pulse and was determined as ~0.93 using Bloch equations simulation of the inversion pulse in predefined T_1/T_2/B0/B1 regimes.[21]

FITTING PROCESS. The same fitting process was used for both models. Prior to dictionary matching, the signal polarity of the measured signal was restored using a phase sensitive inversion recovery (PSIR) reconstruction approach.[22] The first image with the shortest TI (TI_1 = 100 msec) was selected as the reference phase image and was assumed to have "negative" polarity. Based on Bloch equations simulation, this assumption has been shown to be valid for any T_1 time >172 msec (in the presence of any T_2 time ≥30 msec and imaging flip angle ≤85°).[21] Since both signal dictionaries are normalized, the polarity-restored measured signal S_{meas} was individually scaled to each dictionary entry S_{dict} as:

$$S_{meas}^{(scaled)} = S_{meas} \cdot \frac{\overline{|S_{dict}|}}{\overline{|S_{meas}|}}, \quad (2)$$

where $\overline{|S_{dict}|}$ is the signal amplitude average of a dictionary entry over all TIs (ie, TI_1 and TI_2) and $\overline{|S_{meas}|}$ is the signal amplitude average of the polarity-restored measured signal over all TIs (ie, TI_1 and TI_2). Dictionary matching was finally performed by minimizing the L2-norm between $S_{meas}^{(scaled)}$ and each dictionary entry. Graphic processing unit (GPU) implementation of both the dictionary creation and fitting process was developed using the compute unified device architecture (CUDA) (NVIDIA, Quadro K620 2GB) to enable fast T_1 map reconstruction. For comparison, a standard central processing unit (CPU)-based implementation was also developed.

HR CORRECTION. The IR model led to substantial T_1-dependence on HR.[21] Therefore, T_1 estimates obtained from this model were HR-corrected as in previous work[21] and summarized in the Supplementary Materials. No HR correction was performed for the BS model.

Monte Carlo Simulation

Monte Carlo simulation (N = 50,000 repetitions) was performed to investigate T_1/T_2-dependent T_1 accuracy and precision of FAST1-BS, FAST1-IR, and standard 5-(3)-3 MOLLI. The signal of FAST1 and MOLLI was generated using Bloch equations simulation with the following parameter ranges: T_1 ([200,2000] msec in steps of 25 msec), and T_2 ([30,70] msec in steps of 5 msec). Random Gaussian noise was introduced to simulate a typical signal-to-noise ratio (SNR) of 50 in the longest TI image of the MOLLI sequence. T_1 accuracy was calculated as the average over all repetitions of the difference between estimated and actual T_1 times. T_1 precision was measured as the standard deviation (SD) over all repetitions of the estimated T_1 times.

Experimental Evaluation

All imaging experiments were performed using a 1.5T MRI scanner (Magnetom Aera, Siemens Healthcare, Erlangen, Germany). FAST1-BS and FAST1-IR were compared with the standard MOLLI sequence (5-(3)-3 scheme) in phantom, in healthy volunteers as well as in patients. The in vivo studies were approved by a local Research Ethics Committee (approval number 01/11/12 for the healthy volunteer study and approval number 15/NS/0030 for the patient study), with written informed consent obtained from all participants.

PHANTOM EXPERIMENTS. FAST1-BS, FAST1-IR, and MOLLI were initially compared in a phantom (T1MES, Resonance Health, Burswood, WA, Australia) with six vials of different T_1/T_2 times representing typical ranges of native and postcontrast myocardial T_1 times.[23] Both FAST1 and MOLLI sequences were acquired using the same single-shot 2D balanced steady-state free-precession (bSSFP) readout: repetition time (TR)/ echo time (TE)/ flip angle 2.70 msec/1.12 msec/35°, field of view (FOV) 360 × 306 mm^2, acquisition matrix 256 × 144, acquired pixel size 1.4 × 2.1 mm^2, reconstructed pixel size 1.4 × 1.4 mm^2, slice thickness/gap 8/16mm,

GRAPPA acceleration factor 2, partial Fourier factor 7/8, bandwidth 1085 Hz/px, TI_1 100 msec. Five slices were acquired using FAST1, while a single slice (the central slice in FAST1) was acquired using MOLLI. Additionally, an IR spin echo (SE) experiment was performed on another day to obtain reference T_1 times using the following parameters: TE/TR = 15/15000 msec, 15 TIs = [50 msec, 100–900 msec in steps of 100 msec, 1000–5000 msec in steps of 1000 msec], pixel size 1.4×1.4 mm^2, slice thickness 5 mm, and bandwidth 130 Hz/px. Data analysis was performed based on vial-wise region of interest (ROI) in the common slice unless stated otherwise.

Experiment #1: Influences of T_{RD} and R_{THK}. FAST1 was acquired multiple times using different values of T_{RD} ([4,10] sec in steps of 1 sec) and R_{THK} ([2,8] in steps of 1). A simulated HR of 60 bpm was used for this experiment. The maximum interslice T_1 variation ($\max(|\Delta_{SLICE}T_1|)$) was measured for each set of parameters to identify potential slice crosstalk effects. An empirically optimized pair of T_{RD} (6 sec) and R_{THK} (4) was used for FAST1 in all the following experiments in phantom and in vivo.

Experiment #2: HR sensitivity. FAST1 and MOLLI were repeated for different simulated HRs ([40,120] bpm in steps of 10 bpm). Mean T_1 variation across HRs (with respect to T_1 at 60 bpm) was compared for FAST1-BS, FAST1-IR, and MOLLI.

Experiment #3: Characterization of T_1 accuracy, spatial variability, and repeatability. FAST1 and MOLLI were each acquired five times using a simulated HR of 60 bpm. T_1 accuracy, spatial variability, and repeatability were evaluated for FAST1-BS, FAST1-IR, and MOLLI. T_1 accuracy was computed for each vial as the interrepetition average of difference between T_1 mean in ROI and reference T_1 obtained in IR SE experiments. T_1 spatial variability was measured for each vial as the interrepetition average of T_1 SD in ROI. T_1 repeatability was evaluated for each vial as the interrepetition SD of T_1 mean in ROI.

HEALTHY VOLUNTEER EXPERIMENTS. In vivo characterization of native myocardial T_1 mapping using FAST1-BS, FAST1-IR, and MOLLI was performed in nine healthy volunteers (six males, 29 ± 1 years). Both FAST1 and MOLLI were acquired in the short-axis orientation using the imaging parameters described in the phantom experiments with T_{RD} of 6 sec and R_{THK} of 4. FAST1 was acquired three times to cover the entire LV. To this end, the second and third FAST1 acquisitions were positively and negatively shifted in the slice direction by the employed slice thickness, respectively. This thus resulted in the acquisition of 15 contiguous slices covering the entire LV in a total of three separated breathholds. For comparison, three slices were acquired using MOLLI in another three separated breathholds, matching the three central slices in the first FAST1 acquisition, mimicking a conventional clinical MOLLI protocol.

This entire protocol was performed twice within the same session without subject repositioning to assess the repeatability of in vivo native myocardial T_1 mapping. Qualitative and quantitative comparisons between both techniques were undertaken in the three common slices (ie, three central slices in the first slice group using FAST1 and three slices using MOLLI).

Qualitative assessment. No data were discarded for the qualitative assessment. Subjective assessment of map quality for FAST1-BS, FAST1-IR, and MOLLI was performed independently by three experienced cardiac MRI readers (M.S.N./J.W./P.D.: >3/4/3 years of cardiac MRI experience) blinded to the techniques. Since blood T_1 times measured with FAST1 and MOLLI are very different (as FAST1 cannot estimate blood T_1 due to the in-flow effect caused by the slice-selective inversion pulses), the assessment was restrained to the evaluation of map quality only within the myocardium for all techniques to ensure that the readers remain blinded to the acquisition techniques. To this end, endocardial and epicardial contours were manually delineated in the first T_1-weighted image of each slice and used to generate a binary mask of the myocardium. The myocardium from each T_1 map was overlaid to the first T_1-weighted image to prevent any bias in the subjective analysis. Each resulting image was then rated using a 4-point-scale scoring system defined as: 1, nondiagnostic: artifacts in >50% of AHA (American Heart Association) myocardial segments[24]; 2, fair: artifacts in >1 segments and ≤50% of segments; 3, good: artifacts in 1 segment; 4, excellent: no artifacts. Artifacts were defined as regions of inhomogeneous myocardial T_1 occurring in areas assessed to be normal tissue.

Quantitative assessment. All data were visually inspected to detect the presence of severe artifacts or motion among the T_1-weighted images. Slices with apparent severe artifacts in any of FAST1-BS, FAST1-IR, and MOLLI were discarded from the quantitative analysis of all techniques in that specific subject. Native T_1 measures, spatial variability, and repeatability of the three techniques were calculated for each AHA myocardial segment.[24] Native T_1 measures were calculated as the interrepetition average of the T_1 mean in a given myocardial segment. Spatial variability was measured as the interrepetition average of the T_1 SD in a given myocardial segment. Repeatability was evaluated as the interrepetition absolute difference of the T_1 mean in a given myocardial segment. Subject-wise T_1 measures, spatial variability, and repeatability were then computed by averaging the segmental values over all nondiscarded segments for each subject. Segment-wise T_1 measures, spatial variability, and repeatability were also computed by averaging the nondiscarded segmental values over all subjects for each myocardial segment. Finally, intersegment variations of native T_1 measures, spatial variability, and repeatability were calculated as the average over all subjects of the intersegment SD of native T_1 measures, spatial variability, and repeatability, respectively.

PATIENT EXPERIMENTS. Seventeen consecutive patients (eleven males, 51 ± 17 years) referred for cardiac MRI examination in our center were recruited. The clinical indication for the study included cardiomyopathy (twelve patients), assessment of volumes and function (two patients), assessment for aortopathy (two patients), and investigation of myocarditis (one patient). Native and postcontrast myocardial T_1 mapping were performed in the short-axis orientation using FAST1 (15 contiguous slices covering the entire LV in three separated breathholds) and MOLLI (three slices in three separated breathholds, the same as the three central slices in the first slice group of FAST1). Imaging parameters were as described as in the healthy volunteer experiments. Thirteen of these patients (eight males, 51 ± 17 years) received an injection of

0.1 mmol/kg of gadobutrol (Gadovist, Bayer Vital, Leverkusen, Germany) in which postcontrast T_1 mapping was also performed using FAST1 and MOLLI with the protocol described above.

Qualitative assessment. Subjective assessment of map quality was performed for native T_1 maps as described above for the healthy volunteer study.

Quantitative assessment. Subject-wise native and postcontrast T_1 measures were assessed using FAST1-BS, FAST1-IR, and MOLLI, as described in the healthy volunteer study.

Statistical Analysis

Data are expressed as mean ± SD. the Kruskal–Wallis test was used to evaluate the null hypothesis that there is no difference in in vivo subjective map quality scores between FAST1-BS, FAST-IR, and MOLLI, with statistical significance defined at $P < 0.05$. When the Kruskal–Wallis test found statistical significance, Wilcoxon signed rank tests with Bonferroni correction were performed for each pair of techniques, with statistical significance threshold of $P < 0.05/3 = 0.0167$. Interreader variability was assessed using a two-way mixed single-measure intraclass correlation coefficient (ICC).

A one-way analysis of variance (ANOVA) test was used to evaluate the null hypothesis that there is no difference between the three techniques in terms of myocardial T_1 times in healthy volunteers, with statistical significance defined at $P < 0.05$. When the ANOVA test found statistical significance, Student's *t*-tests with Bonferroni correction were performed for each pair of techniques, with statistical significance threshold of $P < 0.05/3 = 0.0167$. The same methodology was used for analysis of myocardial T_1 spatial variability and T_1 repeatability in healthy subjects, as well as for analysis of native and postcontrast myocardial T_1 times in patients.

Pearson correlation and Bland–Altman analyses were also performed between each of the two FAST1 techniques and MOLLI in terms of subject-wise native/postcontrast myocardial T_1 times. Bland–Altman 95% limits of agreement were calculated as the mean difference between methods ±1.96 × (SD of differences).

Results

Reconstruction Time

For a single T_1 map with a matrix size of 256 × 256, T_1 map reconstruction of FAST1-BS/FAST1-IR took 6.5 sec using CPU implementation and 0.2 sec using GPU implementation. The reconstruction time of an entire FAST1-BS/FAST1-IR dataset (ie, five slices) was reduced from 31 sec using CPU implementation to 0.6 sec using GPU implementation. The reconstruction time of three FAST1-BS/FAST1-IR datasets for full LV coverage (ie, 15 slices in three slices groups) was reduced from 94 sec using CPU implementation to 1.4 sec using GPU implementation.

Monte Carlo Simulation

Fig. 2 shows the impact of T_2 on the T_1 accuracy and precision of FAST1-BS, FAST1-IR, and MOLLI. FAST1-BS led to higher accuracy (mean error: 0.2%) than FAST1-IR (mean error: 6%) and MOLLI (mean error: 4%). All techniques were T_2-dependent. Over the entire studied range of T_1 and T_2 times, FAST1-BS and FAST-IR led to reduced precision with respect to MOLLI by factors of 1.7 and 1.5, respectively.

Phantom Experiments

Experiment #1: Influences of T_{RD} and R_{THK}. Maximum interslice T_1 variation ($\max(|\Delta_{SLICE}T_1|)$) as a function of T_{RD} and R_{THK} is shown in Fig. 3. For both FAST1-BS and FAST1-IR, large interslice T_1 variations of up to 62 msec were observed using a short T_{RD} of 4 sec, while maximum interslice T_1 variations were substantially reduced to less than 11 msec for T_{RD} exceeding 6 sec. For both techniques, large maximum interslice variations of up to 204 msec were observed using a large R_{THK} of at least 7, while maximum interslice T_1 variations were substantially reduced to less than 11 msec for R_{THK} not exceeding 4.

Experiment #2: HR sensitivity. Mean T_1 variation across HRs obtained using FAST1-BS, FAST1-IR, and MOLLI are shown in the Supplementary Materials. All techniques demonstrated minimal HR dependence with mean T_1 variations across all HRs <13 msec for all vials and all techniques.

Experiment #3: Characterization of T_1 accuracy, spatial variability, and repeatability. T_1 accuracy, spatial variability, and repeatability of FAST1-BS, FAST1-IR, and MOLLI are shown in Fig. 4. FAST1-BS, FAST1-IR, and MOLLI led to T_1 error of –26 ± 5 msec vs. –73 ± 53 msec vs. –56 ± 36 msec (mean error: 4% vs. 9% vs. 7%), T_1 spatial variability of 9 ± 6 msec vs. 8 ± 4 msec vs. 6 ± 4 msec (mean penalty factors of FAST1-BS/IR with respect to MOLLI: 1.5/1.4) and T_1 repeatability of 1.6 ± 0.8 msec vs. 1.4 ± 0.6 msec vs. 0.8 ± 0.3 msec, respectively.

Healthy Volunteer Experiments

HR among all healthy volunteers was 66 ± 9 bpm ([51,78] bpm). Breathhold length using FAST1 among all healthy volunteers was 12 ± 1 sec. Example T_1 maps obtained using FAST1-BS, FAST1-IR, and MOLLI in one healthy volunteer are shown in Fig. 5. The three techniques provided similar visual map quality across all slices and myocardial segments. Over all subjects, no statistically significant differences were found between subjective map quality obtained using FAST1-BS, FAST1-IR, and MOLLI for each reader (reader #1: 3.3 ± 0.7 vs. 3.6 ± 0.6 vs. 3.4 ± 0.8, respectively, $P = 0.48$; reader #2: 3.4 ± 0.7 vs. 3.6 ± 0.5 vs. 3.6 ± 0.6, respectively, $P = 0.49$; reader #3: 3.6 ± 0.6 vs. 3.9 ± 0.4 vs. 3.7 ± 0.6, respectively, $P = 0.23$; ICC = 0.66).

Among all healthy volunteers, no slices were excluded due to severe artifact level from the data analysis of FAST1-BS, FAST1-IR, and MOLLI. Fig. 6 shows the comparison of the three techniques in terms of subject-wise analysis of native myocardial T_1 times, spatial variability, and repeatability. Each technique led to different native myocardial T_1 times (FAST1-BS: 1016 ± 27 msec, FAST-IR: 952 ± 22 msec, MOLLI: 987 ± 23 msec, $P < 0.0001$) and spatial variability (FAST1-BS: 66 ± 10 msec, FAST-IR:

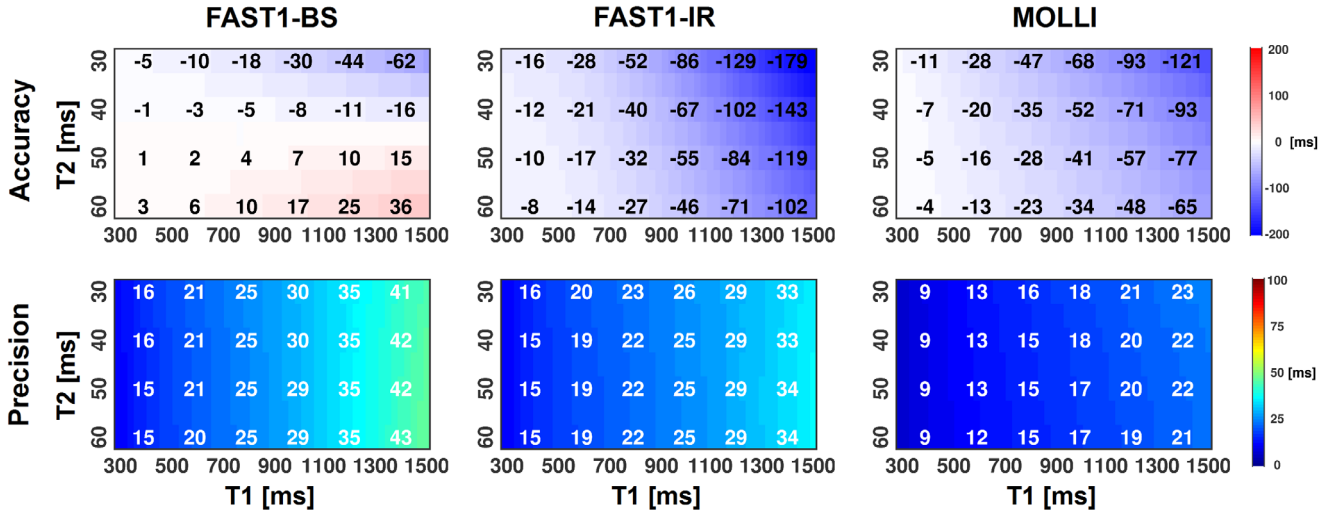

FIGURE 2: Accuracy and precision of FAST1-BS, FAST1-IR, and MOLLI in numerical simulation. FAST1-BS provided higher accuracy and reduced precision than FAST1-IR and MOLLI. FAST1-IR led to reduced accuracy and precision when compared with MOLLI. All techniques were T_2-dependent.

57 ± 8 msec, MOLLI: 46 ± 7 msec, $P < 0.001$). Spatial variability increases of FAST1-BS and FAST1-IR with respect to MOLLI were by factors of 1.4 and 1.2, respectively. There were no statistically significant differences between all techniques in terms of T_1 repeatability (FAST1-BS: 18 ± 6 msec, FAST1-IR: 16 ± 5 msec, MOLLI: 14 ± 5 msec, $P = 0.18$).

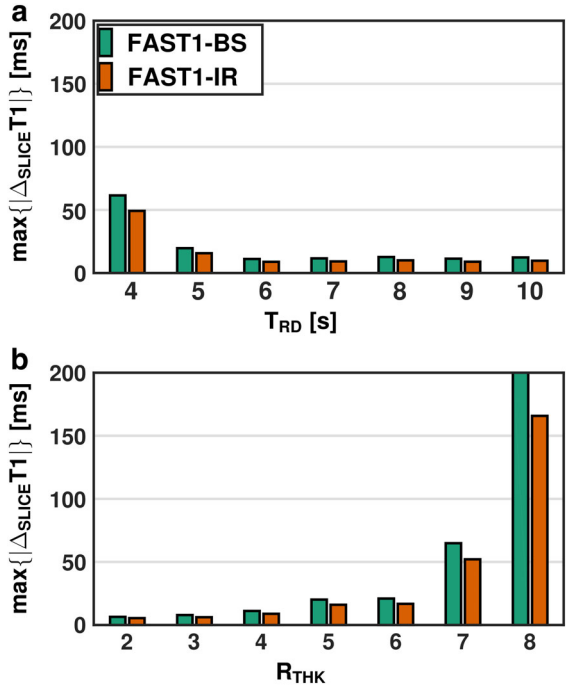

FIGURE 3: Slice crosstalk using different T_{RD} and R_{THK} using FAST1-BS and FAST1-IR in phantom. (a) Maximum interslice T_1 variations among all vials using different T_{RD} from 4 sec to 10 sec and a fixed R_{THK} of 4. With T_{RD} exceeding 6 sec, maximum interslice T_1 variations were restricted to <13 msec. (b) Maximum interslice T_1 variations among all vials using different R_{THK} from 2 to 8 and a fixed T_{RD} of 6 sec. With R_{THK} not exceeding 4, maximum interslice T_1 variations were restricted to <11 msec.

Myocardial segment-based analysis is shown in Fig. 7. There were no statistically significant differences between FAST1-BS, FAST1-IR, and MOLLI in terms of segmental variations of native T_1 measures (31 ± 9 msec vs. 25 ± 7 msec vs. 24 ± 8 msec, respectively, $P = 0.20$), segmental variations of T_1 spatial variability (13 ± 2 msec vs. 11 ± 2 msec vs. 12 ± 4 msec, $P = 0.32$), and segmental variations of T_1 repeatability (13 ± 6 msec vs. 11 ± 5 msec vs. 11 ± 6 msec, $P = 0.58$).

Patient Experiments

HR among all patients was 68 ± 12 bpm ([52,92] bpm). Breathhold length using FAST1 among all patients was 12 ± 2 sec. Figs. 8 and 9 show example native and post-contrast T_1 maps obtained using FAST1-BS, FAST1-IR, and MOLLI in a 31-year-old male patient admitted for suspected myocarditis. Over all patients, FAST1-BS resulted in higher subjective map quality than MOLLI (reader #1: 3.7 ± 0.5 vs. 3.4 ± 0.8, $P = 0.004$; reader #2: 3.8 ± 0.5 vs. 3.5 ± 0.7, $P = 0.002$; reader #3: 3.4 ± 0.8 vs. 3.2 ± 0.8, $P = 0.20$), although these differences only reached statistical significances for readers #1 and #2. FAST1-IR resulted in higher subjective map quality than MOLLI (reader #1: 3.7 ± 0.5 vs. 3.4 ± 0.8, $P = 0.003$; reader #2: 3.8 ± 0.5 vs. 3.5 ± 0.7, $P = 0.006$; reader #3: 3.6 ± 0.6 vs. 3.2 ± 0.8, $P = 0.0005$). The interreader ICC was 0.58.

No slices in FAST1-BS and FAST1-IR were found with a severe artifact level, while a total of eight slices in MOLLI were identified with severe respiratory motion artifacts (8.9% of 90 slices) and subsequently discarded for all techniques for the quantitative analysis. Native myocardial T_1 times using FAST1-BS, FAST1-IR, and MOLLI were 1057 ± 50 msec, 987 ± 42 msec, and 1036 ± 39 msec, respectively ($P < 0.0001$). On the other hand, there were no statistically significant differences between

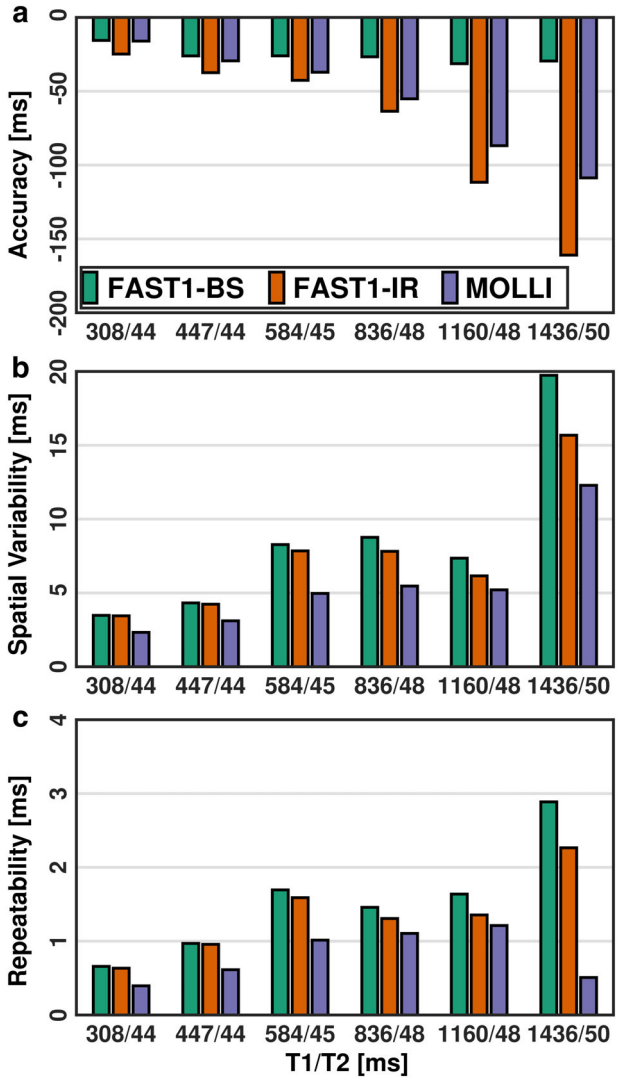

FIGURE 4: T_1 accuracy (a), spatial variability (b), and repeatability (c) of FAST1-BS, FAST1-IR, and MOLLI in phantom. T_1 error was –26 ± 5 msec vs. –73 ± 53 msec vs. –56 ± 36 msec, T_1 spatial variability was 9 ± 6 msec vs. 8 ± 4 msec vs. 6 ± 4 msec and T_1 repeatability was 2 ± 1 msec vs. 1 ± 1 msec vs. 1 ± 0 msec, respectively.

all techniques for postcontrast T_1 times (469 ± 54 msec, 455 ± 52 msec and 454 ± 49 msec, respectively, $P = 0.72$).

Pearson correlation and Bland–Altman analyses of subject-wise native and postcontrast myocardial T_1 times (in healthy volunteers and patients) between FAST1-BS and MOLLI as well as between FAST-IR and MOLLI are shown in Fig. 10. FAST1-BS/FAST1-IR were highly linearly correlated with MOLLI for both native and postcontrast myocardial T_1 estimates (Pearson correlation coefficient = 0.93/0.93 with $P < 0.001$ for native and 0.98/0.98 with $P < 0.001$ for postcontrast). For native myocardial T_1 estimates, FAST1-BS and FAST1-IR led to a bias of 24 ± 18 msec and –44 ± 15 msec with respect to MOLLI, respectively, with a narrow width of 95% limits of agreement (70 msec and 59 msec, respectively). For postcontrast myocardial T_1 estimates, FAST1-BS and FAST1-IR led to a bias of 15 ± 12 msec and 1 ± 11 msec with respect to MOLLI, respectively, with a narrow width of 95% limits of agreement (46 msec and 45 msec, respectively).

Discussion

FAST1 enables multislice myocardial T_1 mapping in one breathhold and full LV coverage in three breathholds. Two FAST1 reconstructions were developed, characterized, and compared with MOLLI in simulation, phantom, healthy volunteers, and patients. The resulting native and postcontrast myocardial T_1 times obtained using FAST1-BS/FAST1-IR and MOLLI showed strong linear correlation. In comparison to MOLLI, FAST1-BS/FAST1-IR led to a 5-fold increase of spatial coverage within the same time frame, limited precision penalty, and no statically significant difference of repeatability.

The sequence parameters T_{RD} and R_{THK} were optimized to ensure the robustness of the sequence in the presence of potential slice crosstalk due to cardiac/respiratory motion and imperfect slice profile with side lobes. T_{RD} was optimized based on normal native myocardial T_1 times at 1.5T. The application of FAST1 at different field strengths or for different tissues of interest may require adjustment of this parameter. The optimized R_{THK} was directly related to the employed imaging slice thickness and slice gap. In this work, R_{THK} of 4, ie, an inversion slice thickness of 32 mm, was found suitable to account for elevated HR. A slice gap of twice the imaging slice thickness was used in this work to avoid gaps or overlaps between slice groups within different breathholds, as we aimed to achieve full LV coverage in three separated breathholds. This parameter should be carefully selected with respect to R_{THK}, the employed imaging slice thickness, and the slice profile of the slice-selective inversion pulse in order to avoid slice crosstalk. The development of a slice-selective inversion pulse with improved slice profile could, however, increase the flexibility of the sequence with respect to these parameters.

In this work, 15 contiguous slices were acquired, which resulted in a spatial coverage of 120 mm in the long-axis dimension. As most hearts are less than 100 mm in the long-axis dimension, slightly reduced coverage may be sufficient for most patients. Although not directly demonstrated in this work, two different strategies could be envisioned to reduce spatial coverage. First, reduced slice thickness/slice gap of 7/14 mm could be used, leading to a total spatial coverage of 15 × 7 mm = 105 mm. Reducing the slice gap could increase the sensitivity of FAST1 to slice crosstalk. However, a small slice gap reduction of 2 mm (from 16 mm to 14 mm) as proposed in this alternative strategy is expected to have minimal impact on slice crosstalk. Reducing the spatial resolution would reduce the SNR in the T_1-weighted images, and thus the precision of T_1 estimates. However, the relative precision penalty of FAST1 with respect to MOLLI is expected to be SNR-independent

based on our previous work using a two-heartbeat T_1 mapping scheme (see Ref. 21, Supplementary Material 6). Alternatively, reduced spatial coverage could be achieved by acquiring only four slices per FAST1 scan (instead of five), which would result in a total spatial coverage of 12 × 8 mm = 96 mm. This could be achieved by discarding the first two heartbeats (ie, slice #1), which would also shorten the required breathholds.

FAST1-BS was more accurate than FAST-IR and MOLLI, which is likely due to its more accurate modeling of the imaging pulses. FAST1-BS was found to be HR-independent. FAST1-IR required the use of a novel HR correction approach to reduce its original HR-dependence.[21] The HR correction designed for FAST1-IR was calibrated using phantom data to provide a method easily translatable to a different scanner. Therefore, it is possible that this model may be suboptimal when applied in vivo. However, the high correlation between FAST1-IR and MOLLI suggests that this correction performed relatively well. Furthermore, FAST1-BS and FAST1-IR may be sensitive to myocardial blood flow due to the use of slice-selective inversion pulses.[25] As FAST1 and MOLLI use analogous acquisition schemes, FAST1-BS and FAST1-IR may also be sensitive to magnetization transfer, which was shown to

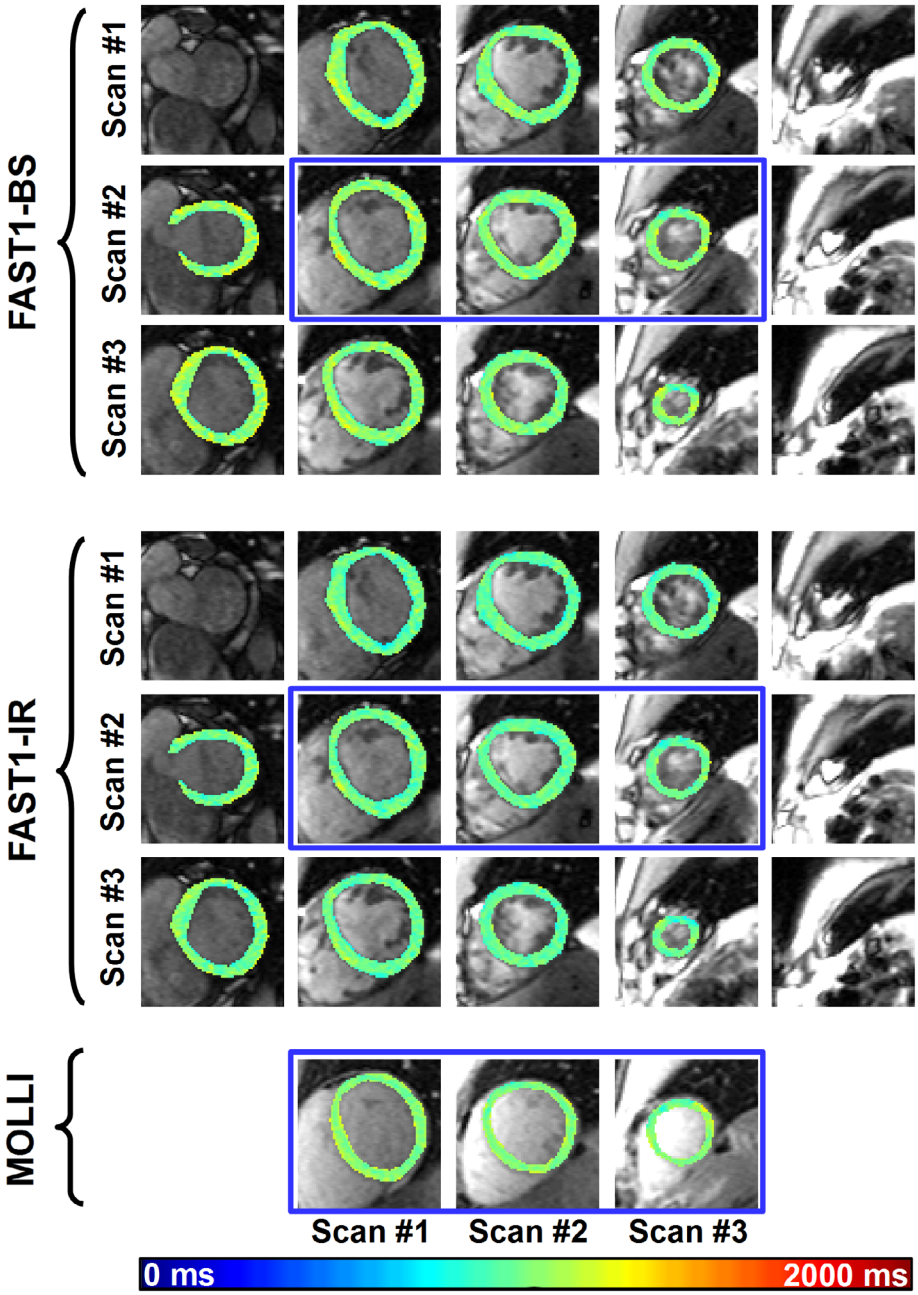

FIGURE 5: Example native myocardial T_1 maps measured in one healthy volunteer using FAST1-BS, FAST1-IR, and MOLLI. Each row for FAST1-BS and FAST1-IR represents one FAST1 acquisition in a separated breathhold. Both FAST1 techniques enabled the acquisition of 15 contiguous slices covering the entire left ventricle in the same time as the acquisition of three slices using MOLLI (ie, 3 breathholds). Note the blue rectangles indicate the three common slice locations in FAST1 and MOLLI.

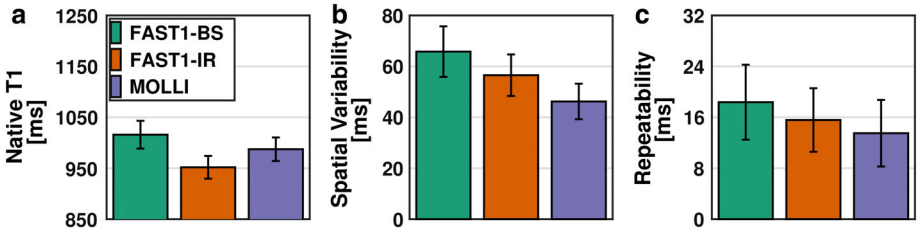

FIGURE 6: Native myocardial T_1 times (a), spatial variability (b), and repeatability (c) using FAST1-BS, FAST1-IR, and MOLLI in healthy volunteers. Average (bar plots) and SD (error bars) over all healthy volunteers are presented. FAST1-BS, FAST1-IR, and MOLLI provided different native myocardial T_1 times ($P < 0.0001$). FAST1-BS and FAST1-IR led to higher spatial variability than MOLLI ($P < 0.001$). There were no statistically significant differences between all techniques for T_1 repeatability ($P = 0.18$).

be the main contributor for the underestimation of in vivo native myocardial T_1 time using MOLLI.[26] FAST1-BS may thus have an advantage over FAST1-IR, as it could enable the integration of the magnetization transfer effect in the creation of the signal dictionary.[27]

T_1 spatial variability is an important criterion for clinical applicability of any T_1 mapping technique. FAST-IR led to an increase of T_1 spatial variability by a factor of 1.2 for in vivo native myocardial T_1 times when compared with MOLLI. This result is in the same order as those reported for the widely used ShMOLLI technique compared with MOLLI for native myocardial T_1 mapping at 1.5T.[6] Since ShMOLLI usually only considers the first five T_1-weighted images only for native myocardial T_1 setting, this suggests that long TI T_1-weighted images have reduced contributions to the precision of T_1 estimates due to their reduced T_1-weighted contrast. FAST1-BS leads to slightly higher increase of T_1 spatial variability (by a factor of 1.4 when compared with MOLLI), but has higher accuracy, as discussed above.

Although FAST1 is based on inversion pulses, this sequence could be modified to use saturation pulses instead. Myocardial T_1 mapping using two images only and a saturation recovery approach has been previously proposed using the arrhythmia insensitive rapid (AIR) T_1 mapping technique, although this technique only enabled the acquisition of one T_1 map per breathhold.[28] A saturation recovery-based FAST1 sequence could be developed using slice-selective saturation pulses or the acquisition of all nonmagnetization prepared images at the beginning of the scan. Nevertheless, AIR was shown to considerably increase the spatial variability of native

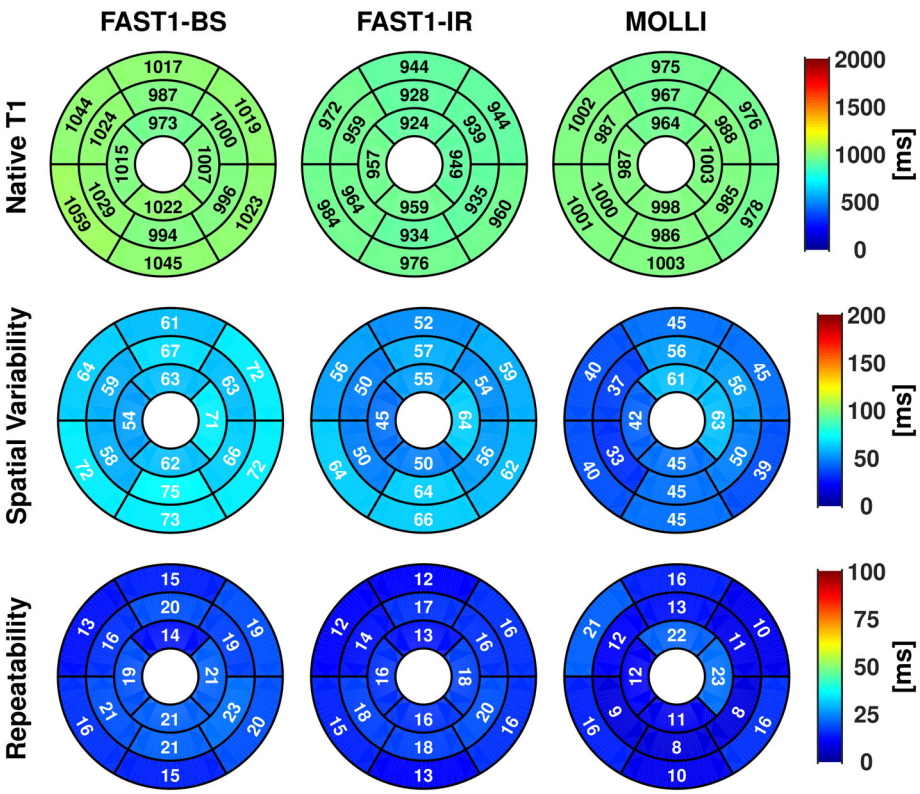

FIGURE 7: Segment-wise native myocardial T_1 measures, spatial variability, and repeatability using FAST1-BS, FAST1-IR, and MOLLI in healthy volunteers. There were no statistically significant differences between all techniques in terms of segmental variations of native T_1 measures ($P = 0.20$), spatial variability ($P = 0.32$), and repeatability ($P = 0.58$).

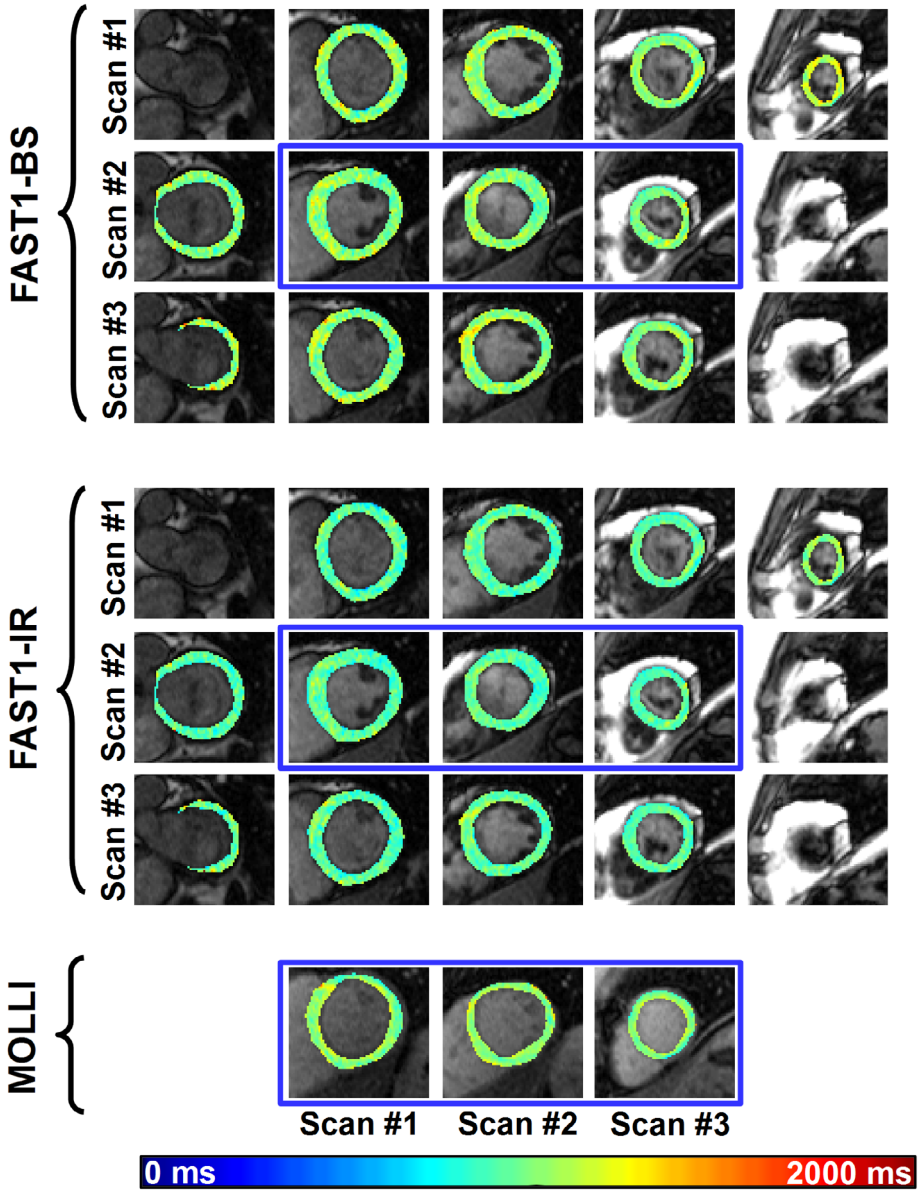

FIGURE 8: Example native myocardial T_1 maps obtained using FAST1-BS, FAST1-IR, and MOLLI in a 31-year-old male patient admitted for suspected myocarditis. Each row for FAST1-BS and FAST1-IR represents one FAST1 acquisition in a separated breathhold. Both FAST1 techniques enabled the acquisition of 15 contiguous slices covering the entire left ventricle in the same time as the acquisition of three slices using MOLLI (ie, three breathholds). Note that the blue rectangles indicate the three common slice locations in FAST1 and MOLLI.

myocardial T_1 mapping by a factor of 2.5 when compared with MOLLI.[29] The proposed IR-based FAST1 approach resulted in a limited increase of spatial variability for native myocardial T_1 mapping by a factor of 1.4 (FAST1-BS) and 1.2 (FAST1-IR) when compared with MOLLI. Furthermore, the HR-independence of FAST1-BS and FAST1-IR also suggests their insensitivity to arrhythmia, as only two images are acquired per slice. Although not directly demonstrated in this study, these findings suggest that an IR-based FAST1 approach may have substantial advantages over a saturation recovery-based FAST1 approach.

In this work, only the short-axis orientation was investigated to minimize the sensitivity to the partial volume effect compared with the other orientations. However, the short-axis orientation is suboptimal for imaging at the apical level, and the use of an additional long-axis slice may be beneficial if mapping of the apex is intended.

Motion correction was not performed for FAST1 and MOLLI. Since each T_1 map is reconstructed from only two images in FAST1 and eight images in MOLLI, it is possible than FAST1 provide better native image registration, which could have potentially explained the slightly reduced T_1 map quality of MOLLI with respect to FAST1 in patients. Existing image registration algorithms may provide different performance based on the number of T_1-weighted images and the presence of an in-flow effect in the LV blood pool such as

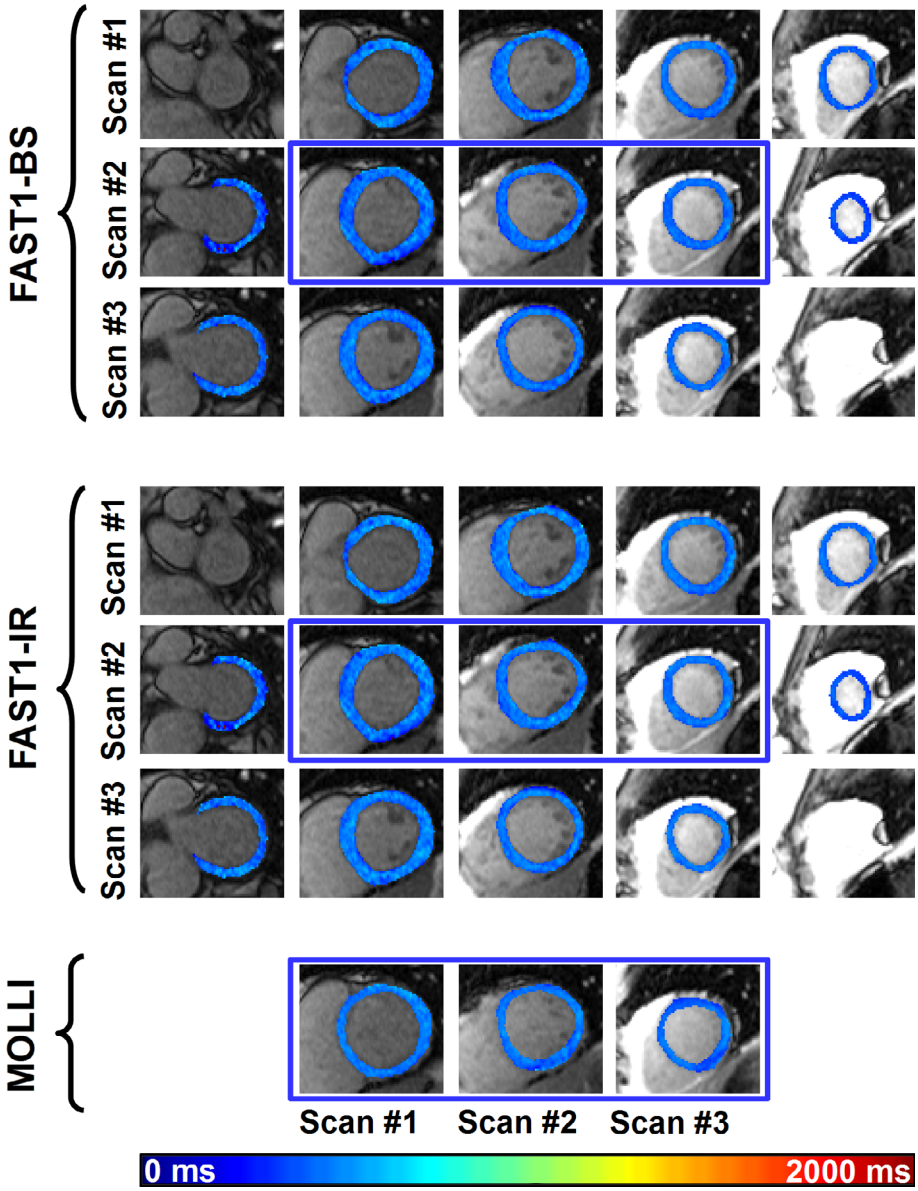

FIGURE 9: Example postcontrast myocardial T_1 maps obtained using FAST1-BS, FAST1-IR, and MOLLI in a 31-year-old male patient admitted for suspected myocarditis. Each row for FAST1-BS and FAST1-IR represents one FAST1 acquisition in a separated breathhold. Both FAST1 techniques enabled the acquisition of 15 contiguous slices covering the entire left ventricle in the same time as the acquisition of three slices using MOLLI (ie, three breathholds). Note the blue rectangles indicate the three common slice locations in FAST1 and MOLLI.

in FAST1. Therefore, to prevent any bias between the techniques induced by the choice of the image registration algorithm, this step was not applied in this work. Nevertheless, image registration algorithms were shown to improve myocardial T_1 map quality.[30,31] Therefore, the development of an image registration step in the FAST1 reconstruction will be investigated in future work.

FAST1 does not allow for quantification of blood T_1 times due to the in-flow effect caused by the slice-selective inversion pulse. Therefore, FAST1 cannot be directly applied for extracellular volume (ECV) quantification. The combination of FAST1 with an additional mid-ventricular T_1 map acquired using nonselective inversion for blood T_1 quantification could enable multislice ECV mapping with FAST1 and will be investigated in future work.

This work was performed at 1.5T. Future work will investigate the feasibility of FAST1 at 3T with the potential benefit for scar assessment in patients with chronic myocardial infarction.[5] Due to the longer native myocardial T_1 times at 3T, a longer T_{RD} may be necessary to achieve nearly full recovery of the longitudinal magnetization. The combination of FAST1 with a gradient recalled echo (GRE) readout could also be beneficial to reduce off-resonance artifacts at higher fields.[32,33]

This work has several limitations. First, the approximation of the slice profile was approximated by one flip angle only. More advanced modeling could be considered in future work to better

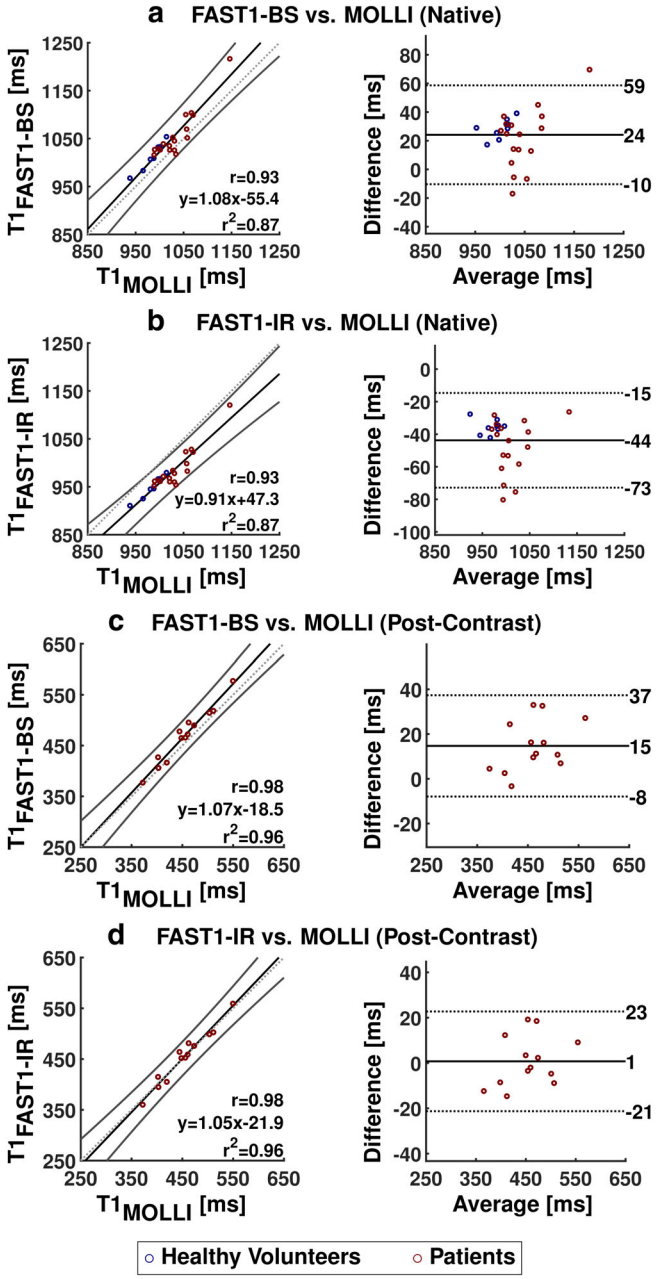

FIGURE 10: Pearson correlation and Bland–Altman analyses between FAST-BS and MOLLI (a,c) as well as between FAST1-IR and MOLLI (b,d) for both native and postcontrast myocardial T_1 times measured in both healthy volunteers and patients. In Pearson correlation analysis plots, confidence interval (solid lines) and identity line (y = x, dashed line) are also plotted besides the linear regression line (solid line). FAST1-BS and FAST1-IR yielded highly linearly correlated T_1 times with MOLLI (Pearson correlation coefficient = 0.93 for native and 0.98 for postcontrast myocardial T_1 times).

represent the nonlinear signal response to the flip angle.[33] Second, postcontrast myocardial T_1 mapping using FAST1 was not characterized in healthy volunteers. However, the phantom and patient experiments demonstrated the feasibility of postcontrast myocardial T_1 mapping using FAST1. Third, no statistical analysis was performed for the phantom study, as only six vials with realistic myocardial T_1 times were available, thus limiting the available power. However, the trend observed in the phantom experiments was confirmed in both numerical simulations and in vivo studies. Finally, the patient study was used for studying feasibility. Further studies in larger patient cohorts are now warranted.

In conclusion, FAST1 enables myocardial T_1 mapping with full LV coverage in three separated breathholds. In comparison with MOLLI, FAST1-BS and FAST1-IR yield a 5-fold increase of spatial coverage, limited penalty of T_1 precision/spatial variability, no significant difference of T_1 repeatability, and highly correlated T_1 times. FAST1-IR provides improved T_1 precision/spatial variability but reduced accuracy when compared with FAST1-BS.

Acknowledgment

Contract grant sponsor Health Innovation Challenge Fund; Contract grant number: HICF-R10-698; Contract grant sponsor: a parallel funding partnership between the Department of Health and the Wellcome Trust, the Wellcome Engineering and Physical Sciences Research Council (EPSRC) Centre for Medical Engineering at King's College London; Contract grant number: WT 203148/Z/16/Z; Contract grant sponsor: EPSRC; Contract grant number: EP/R010935/1; Contract grant sponsor: National Institute for Health Research (NIHR) Biomedical Research Centre award to Guy's and St Thomas' National Health Service (NHS) Foundation Trust in partnership with King's College London, and by the NIHR Healthcare Technology Co-operative for Cardiovascular Disease at Guy's and St Thomas' NHS Foundation Trust.

References

1. Moon JC, Messroghli DR, Kellman P, et al. Myocardial T1 mapping and extracellular volume quantification: A Society for Cardiovascular Magnetic Resonance (SCMR) and CMR Working Group of the European Society of Cardiology consensus statement. J Cardiovasc Magn Reson 2013;15:92.
2. Messroghli DR, Radjenovic A, Kozerke S, Higgins DM, Sivananthan MU, Ridgway JP. Modified Look-Locker inversion recovery (MOLLI) for high-resolution T1 mapping of the heart. Magn Reson Med 2004;52:141–146.
3. Kato S, Nakamori S, Bellm S, et al. Myocardial native T1 time in patients with hypertrophic cardiomyopathy. Am J Cardiol 2016;118: 1057–1062.
4. Messroghli DR, Walters K, Plein S, et al. Myocardial T1 mapping: Application to patients with acute and chronic myocardial infarction. Magn Reson Med 2007;58:34–40.
5. Kali A, Choi EY, Sharif B, et al. Native T1 mapping by 3-T CMR imaging for characterization of chronic myocardial infarctions. JACC Cardiovasc Imaging 2015;8:1019–1030.
6. Piechnik SK, Ferreira VM, Dall'Armellina E, et al. Shortened modified Look-Locker inversion recovery (ShMOLLI) for clinical myocardial T1-mapping at 1.5 and 3 T within a 9 heartbeat breathhold. J Cardiovasc Magn Reson 2010;12:69.
7. Chow K, Flewitt JA, Green JD, Pagano JJ, Friedrich MG, Thompson RB. Saturation recovery single-shot acquisition (SASHA) for myocardial T(1) mapping. Magn Reson Med 2014;71:2082–2095.
8. Weingartner S, Akcakaya M, Basha T, et al. Combined saturation/-inversion recovery sequences for improved evaluation of scar and diffuse fibrosis in patients with arrhythmia or heart rate variability. Magn Reson Med 2014;71:1024–1034.

9. Roujol S, Weingärtner S, Foppa M, et al. Accuracy, precision, and reproducibility of four T1 mapping sequences: A head-to-head comparison of MOLLI, ShMOLLI, SASHA, and SAPPHIRE. Radiology 2014;272:683–689.
10. Teixeira T, Hafyane T, Stikov N, et al. Comparison of different cardiovascular magnetic resonance sequences for native myocardial T1 mapping at 3T. J Cardiovasc Magn Reson 2016;18:65.
11. Kellman P, Hansen MS. T1-mapping in the heart: Accuracy and precision. J Cardiovasc Magn Reson 2014;16:2.
12. Weingärtner S, Meßner NM, Budjan J, et al. Myocardial T 1-mapping at 3T using saturation-recovery: Reference values, precision and comparison with MOLLI. J Cardiovasc Magn Reson 2017;18:84.
13. Kvernby S, Warntjes MJ, Haraldsson H, Carlhall CJ, Engvall J, Ebbers T. Simultaneous three-dimensional myocardial T1 and T2 mapping in one breath hold with 3D-QALAS. J Cardiovasc Magn Reson 2014;16:102.
14. Coniglio A, Di Renzi P, Vilches Freixas G, et al. Multiple 3D inversion recovery imaging for volume T1 mapping of the heart. Magn Reson Med 2013;69:163–170.
15. Clique H, Cheng HLM, Marie PY, Felblinger J, Beaumont M. 3D myocardial T1 mapping at 3T using variable flip angle method: Pilot study. Magn Reson Med 2014;71:823–829.
16. Weingärtner S, Roujol S, Akçakaya M, Basha TA, Nezafat R. Free-breathing multislice native myocardial T1 mapping using the slice-interleaved T1 (STONE) sequence. Magn Reson Med 2015;74:115–124.
17. Nordio G, Henningsson M, Chiribiri A, Villa AD, Schneider T, Botnar RM. 3D myocardial T1 mapping using saturation recovery. J Magn Reson Imaging 2017;46:218–227.
18. Chen Y, Lo WC, Hamilton JI, et al. Single breath-hold 3D cardiac T1 mapping using through-time spiral GRAPPA. NMR Biomed 2018;31:e3923.
19. Guo R, Chen Z, Wang Y, Herzka DA, Luo J, Ding H. Three-dimensional free breathing whole heart cardiovascular magnetic resonance T 1 mapping at 3 T. J Cardiovasc Magn Reson 2018;20:64.
20. Mehta BB, Chen X, Bilchick KC, Salerno M, Epstein FH. Accelerated and navigator-gated look-locker imaging for cardiac t1 estimation (ANGIE): Development and application to T1 mapping of the right ventricle. Magn Reson Med 2015;73:150–160.
21. Huang L, Neji R, Nazir MS, et al. Fast myocardial T1 mapping using shortened inversion recovery based schemes. Journal of Magnetic Resonance Imaging 2019 [Epub ahead of print].
22. Xue H, Greiser A, Zuehlsdorff S, et al. Phase-sensitive inversion recovery for myocardial T1 mapping with motion correction and parametric fitting. Magn Reson Med 2013;69:1408–1420.
23. Captur G, Gatehouse P, Keenan KE, et al. A medical device-grade T1 and ECV phantom for global T1 mapping quality assurance—The T1 Mapping and ECV Standardization in cardiovascular magnetic resonance (T1MES) program. J Cardiovasc Magn Reson 2016;18:58.
24. Cerqueira MD, Weissman NJ, Dilsizian V, et al. American Heart Association Writing Group on Myocardial S, Registration for Cardiac I. Standardized myocardial segmentation and nomenclature for tomographic imaging of the heart. A statement for healthcare professionals from the Cardiac Imaging Committee of the Council on Clinical Cardiology of the American Heart Association. Circulation 2002;105:539–542.
25. Keith GA, Rodgers CT, Chappell MA, Robson MD. A Look-Locker acquisition scheme for quantitative myocardial perfusion imaging with FAIR arterial spin labeling in humans at 3 Tesla. Magn Reson Med 2017;78:541–549.
26. Robson MD, Piechnik SK, Tunnicliffe EM, Neubauer S. T1 measurements in the human myocardium: The effects of magnetization transfer on the SASHA and MOLLI sequences. Magn Reson Med 2013;70:664–670.
27. Malik SJ, Teixeira RPA, Hajnal JV. Extended phase graph formalism for systems with magnetization transfer and exchange. Magn Reson Med 2018;80:767–779.
28. Fitts M, Breton E, Kholmovski EG, et al. Arrhythmia insensitive rapid cardiac T1 mapping pulse sequence. Magn Reson Med 2013;70:1274–1282.
29. Hong K, Kim D. MOLLI and AIR T1 mapping pulse sequences yield different myocardial T1 and ECV measurements. NMR Biomed 2014;27:1419–1426.
30. Xue H, Shah S, Greiser A, et al. Motion correction for myocardial T1 mapping using image registration with synthetic image estimation. Magn Reson Med 2012;67:1644–1655.
31. Roujol S, Foppa M, Weingartner S, Manning WJ, Nezafat R. Adaptive registration of varying contrast-weighted images for improved tissue characterization (ARCTIC): Application to T1 mapping. Magn Reson Med 2015;73:1469–1482.
32. Jang J, Bellm S, Roujol S, et al. Comparison of spoiled gradient echo and steady-state free-precession imaging for native myocardial T1 mapping using the slice-interleaved T1 mapping (STONE) sequence. NMR Biomed 2016;29:1486–1496.
33. Shao J, Rapacchi S, Nguyen KL, Hu P. Myocardial T1 mapping at 3.0 tesla using an inversion recovery spoiled gradient echo readout and Bloch equation simulation with slice profile correction (BLESSPC) T1 estimation algorithm. J Magn Reson Imaging 2016;43:414–425.